Isomeric bipyridine-based covalent organic frameworks for efficient electrocatalytic nitrate reduction to ammonia

Shuanglong Lu*, Fulin Yang, Hongyin Hu, Donghua Li, Hailong Hu, Jinyan Wang, Fang Duan, Mingliang Du

Key Laboratory of Synthetic and Biological Colloids, Ministry of Education, School of Chemical and Material Engineering, Jiangnan University, Wuxi, Jiangsu 214122, P. R. China.

Experimental section

Materials

The compounds 4,4′,4″,4‴-(pyrene-1,3,6,8-tetrayl)-tetraaniline (Py), 2,2′-bipyridyl-5,5′-dialdehyde (Bpy), and 3,3′-bipyridine-6,6′-dicarboxaldehyde (PyIm) were obtained from Jilin Chinese Academy of Sciences-Yanshen Technology Co. Solvents such as 1,4-dioxane, mesitylene, acetic acid (AcOH), tetrahydrofuran, ethanol, methanol, and isopropanol were sourced from Shanghai Civi Chemical Technology Co. Potassium hydroxide (KOH), potassium nitrate (KNO_3), Nafion solution, metal acetates ($M(CH3COOH)_2$, where M = Fe, Co, or Ni), and carbon support were acquired from Aladdin Industrial Co. Deionized water (approximately 18.42 MΩ·cm resistivity) was used to prepare electrolyte solutions. All solvents were used as supplied, without further purification.

Characterizations

Sample morphology and structure were examined using field-emission scanning electron microscopy (SEM) with elemental analysis (S-4800) and transmission electron microscopy (TEM) (JEM-2100plus). Aberration-corrected high-angle annular dark-field scanning transmission electron microscopy (HAADF-STEM) was conducted on a FEI Themis Z microscope (Titan Cubed Themis G2300). Powder X-ray diffraction (PXRD) analysis was performed on a Bruker DAVINCI diffractometer with Cu Kα radiation. X-ray photoelectron spectroscopy (XPS) was carried out using a Thermo Scientific K-Alpha spectrometer, and Fourier-transform infrared (FT-IR) spectra were recorded on a Nicolet 6700 spectrometer. Metal concentrations in samples were determined by inductively coupled plasma atomic emission spectrometry (ICP-AES) with a PerkinElmer 8300. The Brunauer–Emmett–Teller (BET) specific surface area was measured by nitrogen adsorption at 77 K using an ASAP2020 MP surface area analyzer.

Synthesis of Py-Bpy-COF, Py-Bpy-M, Py-PyIm-COF and Py-PyIm-Fe.

Synthesis of Py-Bpy-COF: In a 10 mL Pyrex tube, Py (85.07 mg, 0.15 mmol), Bpy (64.01 mg, 0.30 mmol), mesitylene (1.5 mL), 1,4-dioxane (1.5 mL), and 500 μL of 3 M AcOH solution were added. The mixture was sonicated for five minutes, then flash-frozen in liquid nitrogen and degassed through three cycles of freeze-pump-thaw. The tube was flame-sealed under vacuum with a Schlenk line and oil pump, then heated at 120 °C for 72 hours. Once cooled to room temperature, the orange product was sequentially washed with THF, water, and methanol. The resulting powder underwent Soxhlet extraction with THF for 24 hours, was collected, and dried under vacuum at 60 °C overnight

to yield the target COF.

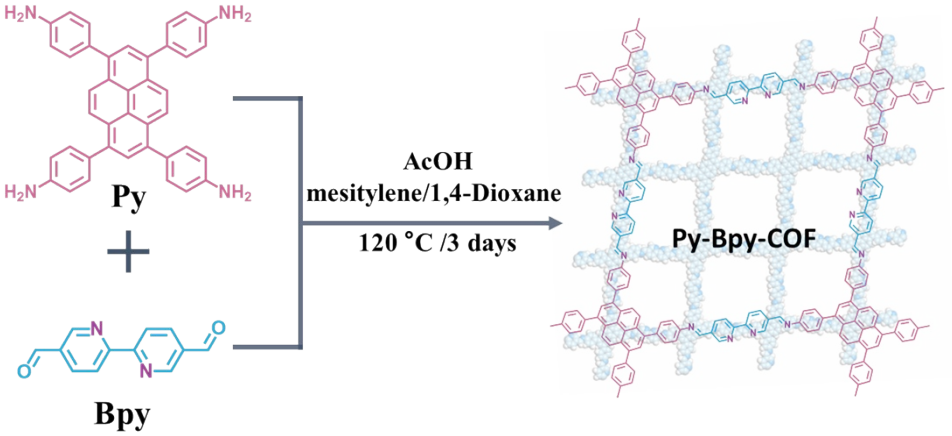

Schematic synthesis of Py-Bpy-COF.

Synthesis of Py-Bpy-M: A mixture of Py-Bpy-COF (20 mg) and $M(OAc)_2$ (10 mg) was prepared in 20 mL of methanol and then refluxed for 12 hours. The resulting solid was filtered, washed with methanol, and dried under vacuum at 60 °C overnight, yielding Py-Bpy-M (M =Fe, Co or Ni).

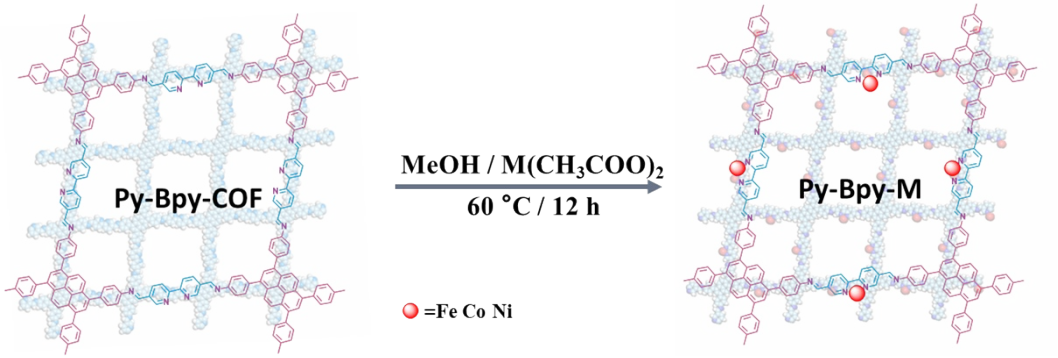

Schematic synthesis of Py-Bpy-M.

Synthesis of Py-PyIm-COF: In a 10 mL Pyrex tube, a mixture of mesitylene, dioxane, and 6 M AcOH (5/5/1 by volume; 1.1 mL) was combined with Py-NH2 (11.3 mg, 0.02 mmol) and 3,3′-Bpy (8.5 mg, 0.04 mmol). The mixture was degassed using three freeze-pump-thaw cycles, then the tube was sealed and heated at 120 °C for 72 hours. After cooling, the precipitate was separated by centrifugation and washed with anhydrous THF and acetone. The resulting powder was dried under vacuum at 120 °C overnight to obtain the Py-PyIm-COF.

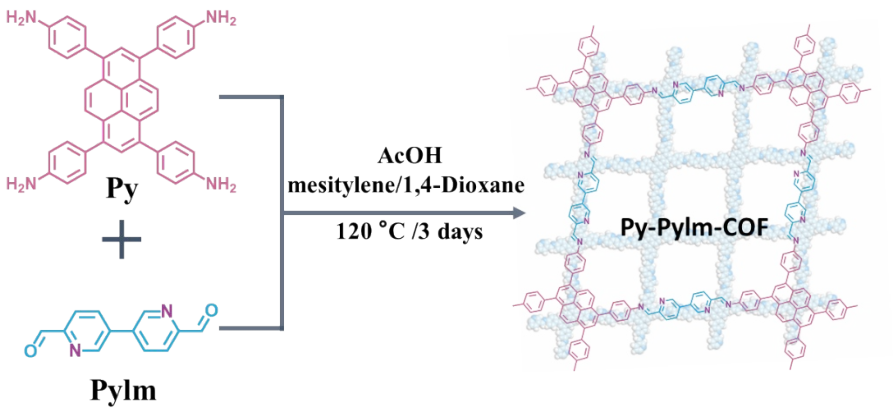

Schematic synthesis of Py-PyIm-COF.

Synthesis of Py-PyIm-Fe: A mixture of Py-PyIm-COF (20 mg) and $Fe(OAc)_2$ (10 mg) was prepared in 20 mL of methanol and then refluxed for 12 hours. The resulting solid was filtered, washed with methanol, and dried under vacuum at 60 °C overnight, yielding Py-PyIm-Fe.

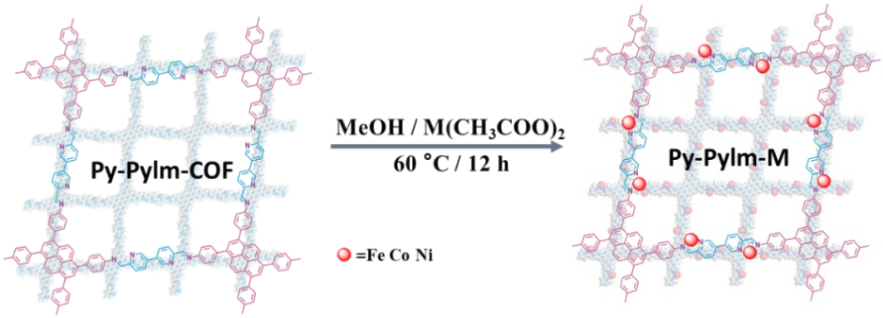

Schematic synthesis of Py-PyIm-Fe.

Electrochemical Measurements.

COFs (2 mg) were dispersed in a solution of isopropyl alcohol (970 μL) and 5 wt% Nafion 117 solution (30 μL) by bath sonication for 30 minutes to create a uniform catalyst ink. A 100 μL portion of this ink was then drop-cast onto a 1×1 cm^2 carbon paper, achieving a catalyst loading of 0.2 mg cm^{-2}.

All electrochemical tests were carried out on a CHI-660H workstation (Shanghai Chenhua) using a typical three-electrode setup. The working electrode was carbon paper coated with the catalyst, while a platinum mesh served as the counter electrode, and a $Hg/HgCl_2$ electrode was used as the reference. NO_3RR measurements, including cyclic voltammetry (CV), linear sweep voltammetry (LSV), and chronoamperometry (i-t), were conducted in an H-cell, where 1 M KOH and 0.1 M KNO_3 acted as the electrolyte. The cell was separated by a pretreated Nafion 117 membrane. Potentiostatic tests were performed at various potentials for 1 hour with a stirring rate of 600 rpm.

To measure the NH_3 Faradaic efficiencies (FE) and yield rates, the potential was varied from −1.4 to −2.0 V vs. SCE in −0.1 V intervals. Isotopic labeling experiments were done under the same conditions at −1.6 V vs. SCE, but using 99% $K^{15}NO_3$ as the nitrogen source.

ECSA was assessed using cyclic voltammetry (CV) at varying scan rates within a potential window free of Faradaic currents. The capacitance, Δj ($0.5\times|j_{charge} - j_{discharge}|$), was plotted against the scan rate, resulting in a straight line. The slope of this line corresponds to the electrochemical double-layer capacitance (C_{dl}). The ECSA of the catalyst is determined by dividing C_{dl} by the specific capacitance (Cs) of the sample.

Determination of product concentration.

Ion concentrations in the pre- and post-test electrolytes were measured using a UV-Vis spectrophotometer after dilution to an appropriate concentration within the calibration curve range. The concentration was determined from the corresponding standard calibration curve. The detection process involved preparing a color reagent by mixing 4 g of p-aminobenzenesulfonamide, 0.2 g of N-(1-Naphthyl) ethylenediamine dihydrochloride, 50 mL of ultrapure water, and 10 mL of phosphoric acid (ρ = 1.70 g/mL). A 2 mL sample of electrolyte was taken, diluted, and 40 μL of the reagent was added. The NO_2^- concentration in an unknown sample was calculated from its absorbance at 540 nm using the calibration curve. Hydrazine (N_2H_4) was measured using the Watt and Chrisps method. A color reagent was prepared by mixing 300 mL of ethanol, 30 mL of concentrated HCl, and 5.99 g of $C_9H_{11}NO$. Two milliliters of this reagent was added to 2 mL of the sample, followed by stirring for 30 minutes at room temperature. The N_2H_4 concentration in the sample was determined from its absorbance at 455 nm and the calibration curve.

NH_3 was measured using the salicylate method, where NH_3 reacts with salicylate and hypochlorite to form indophenol blue. In this procedure, 500 μL of an aqueous solution containing 0.4 M sodium salicylate and 0.32 M sodium hydroxide, 50 μL of sodium hypochlorite solution (approximately 4.5% active chlorine and 0.75 M sodium hydroxide), and 50 μL of a 10 mg/mL sodium nitroferricyanide solution were added sequentially to 3 mL of the sample. The NH_3 concentration in an unknown sample was determined by measuring its absorbance at 655 nm and comparing it to the calibration curve.

2. Supporting figures

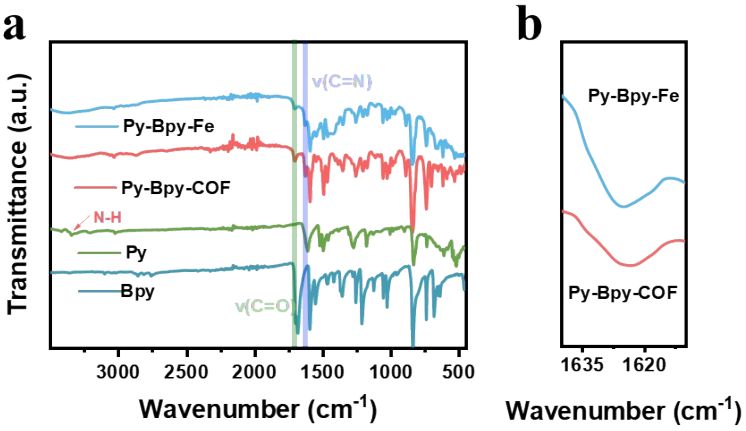

Figure S1. (a) FT-IR spectra of Py, Bpy, Py-Bpy-COF and Py-Bpy-Fe, (b) the marked FT-IR spectra in Fig S1a.

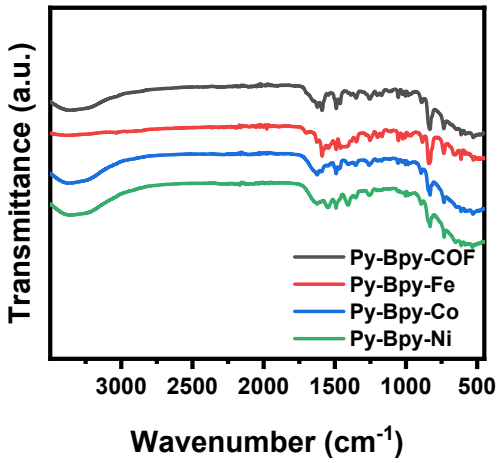

Figure S2. FT-IR spectra of Py-Bpy-COF, Py-Bpy-Fe, Py-Bpy-Co and Py-Bpy-Ni.

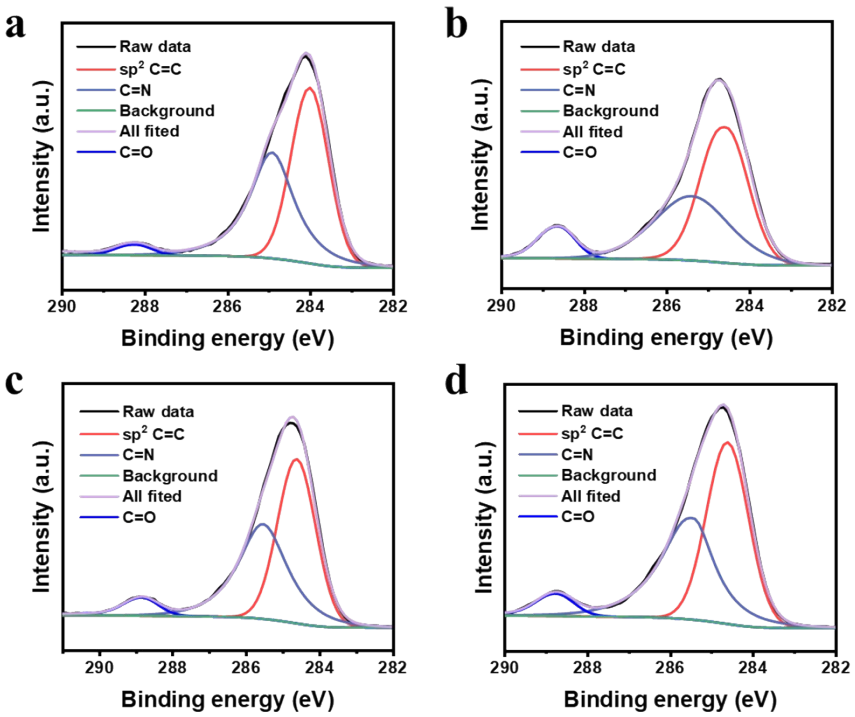

Figure S3. C1s XPS spectra and their deconvolution of (a) Py-Bpy- COF, (b) Py-Bpy-Fe, (c) Py-Bpy-Co, (d) Py-Bpy-Ni.

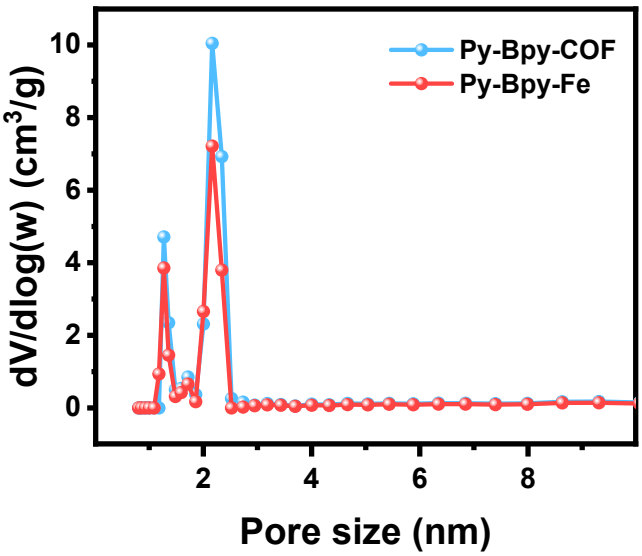

Figure S4. The pore size distribution of Py-Bpy-COF and Py-Bpy-Fe.

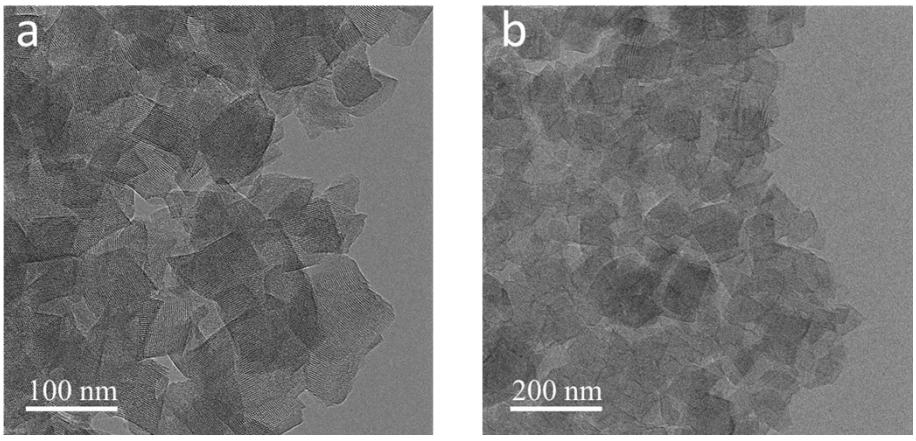

Figure S5. HR-TEM images of Py-Bpy-COF.

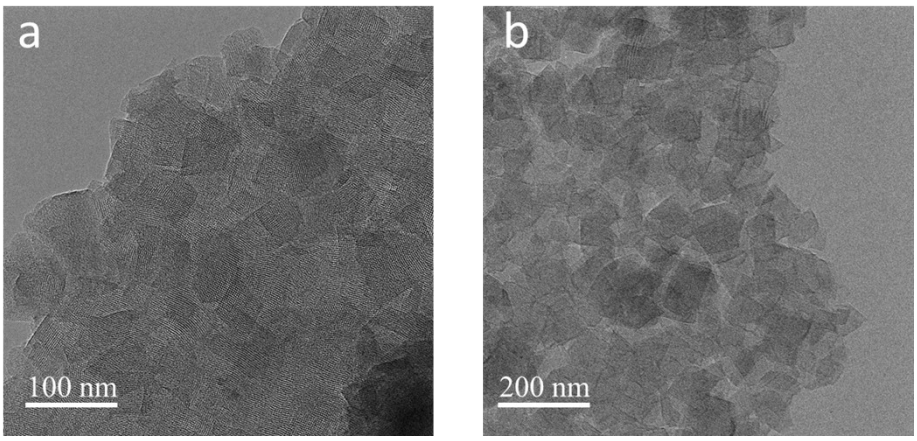

Figure S6. HR-TEM images of Py-Bpy-Fe.

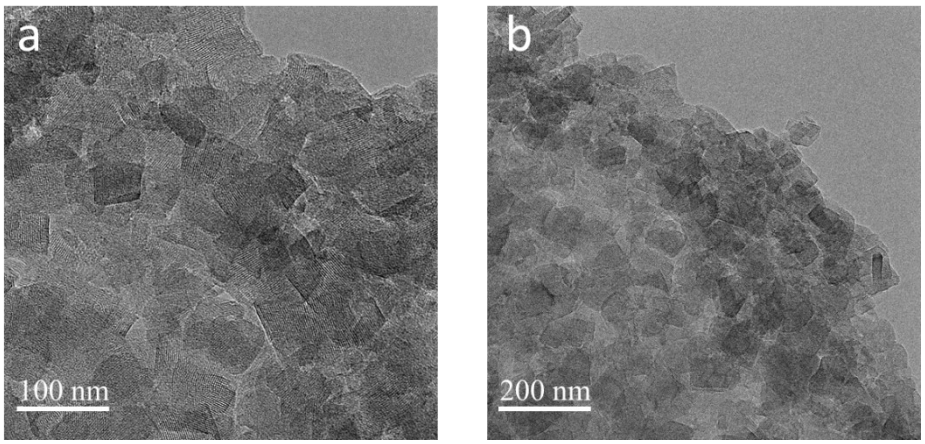

Figure S7. HR-TEM images of Py-Bpy-Co.

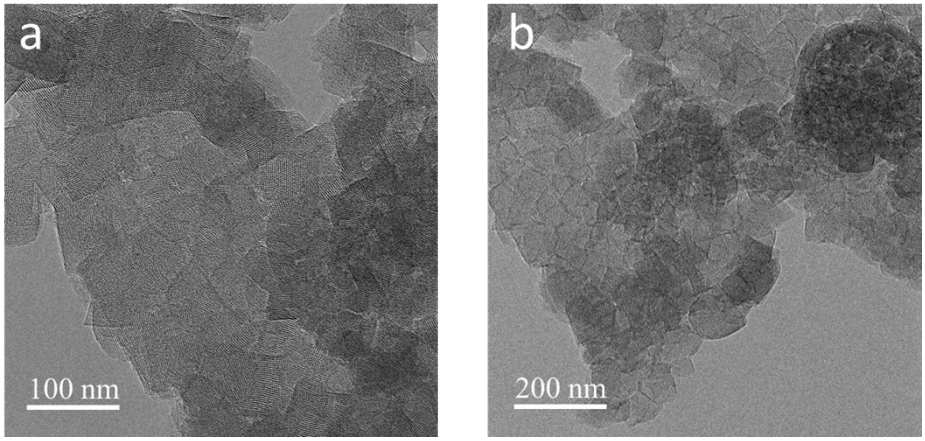

Figure S8. HR-TEM images of Py-Bpy-Ni.

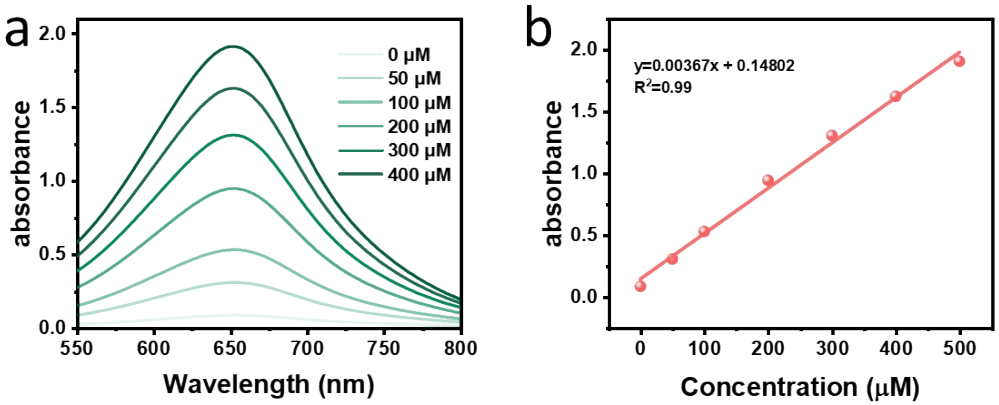

Figure S9. The UV-Vis curves and calibration curves of the electrolyte with the given NH_3 concentrations

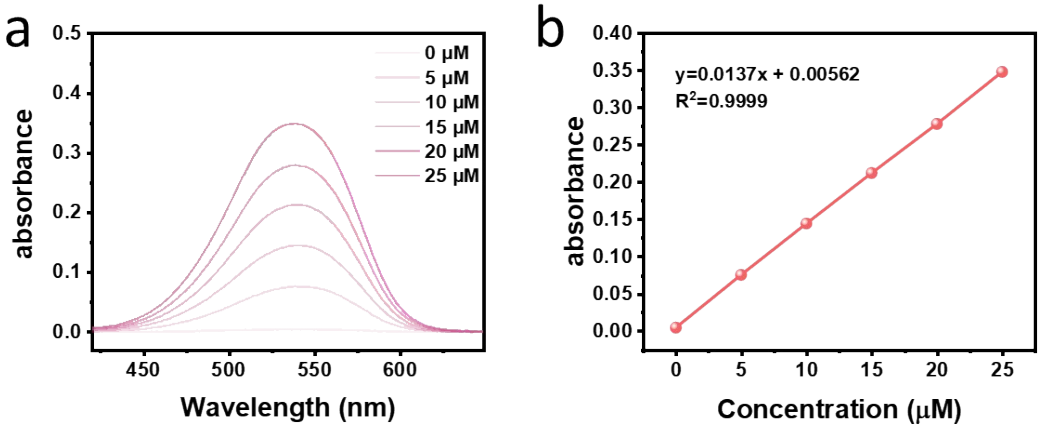

Figure S10. The UV-Vis curves and calibration curves of the electrolyte with the given NO_2^- concentrations

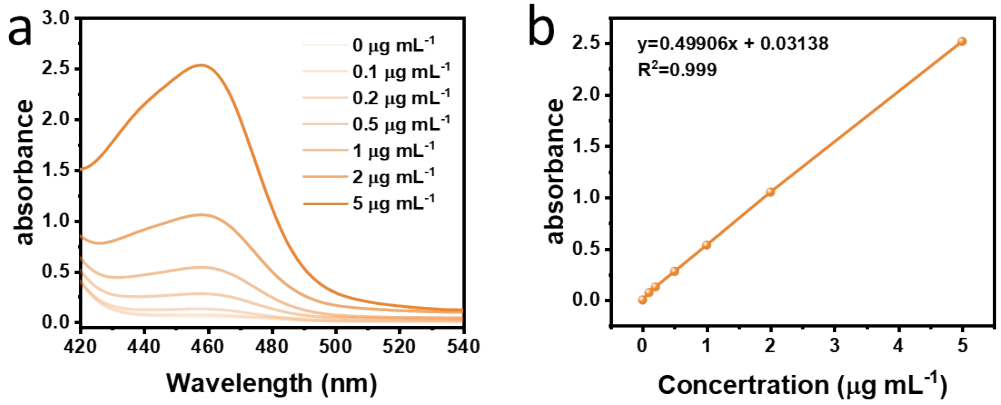

Figure S11. The UV-Vis curves and calibration curves of the electrolyte with the given N_2H_2 concentrations

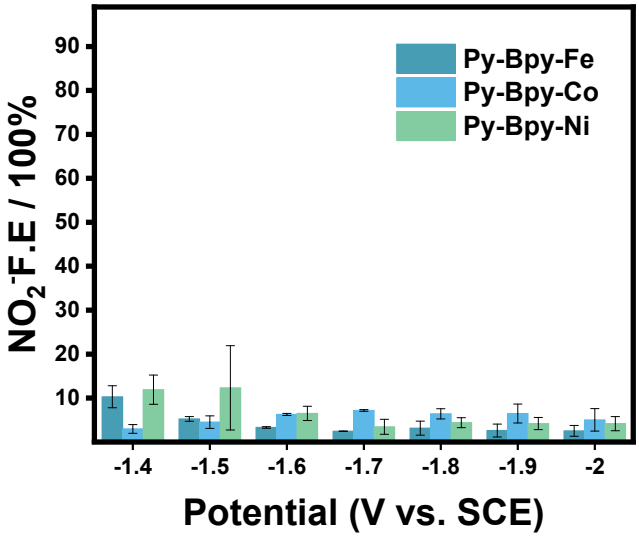

Figure S12. NO_2^- FE of Py-Bpy-Fe, Py-Bpy-Co and Py-Bpy-Ni at each given potential.

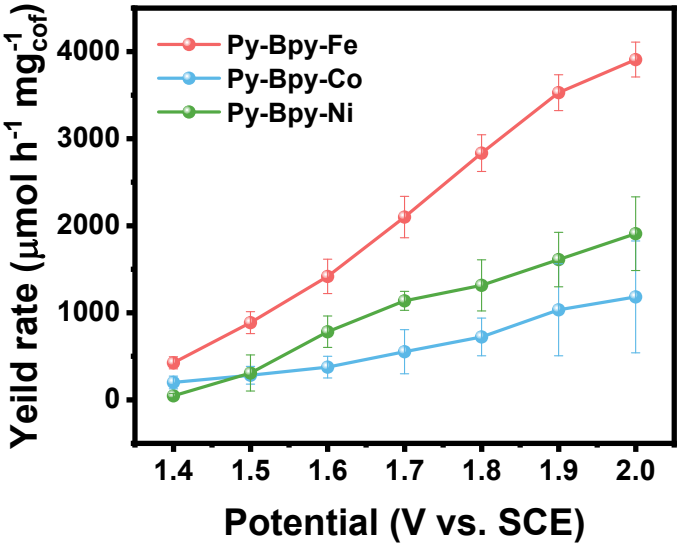

Figure S13. NH_3 yield rate of Py-Bpy-Fe, Py-Bpy-Co and Py-Bpy-Ni at each given potential.

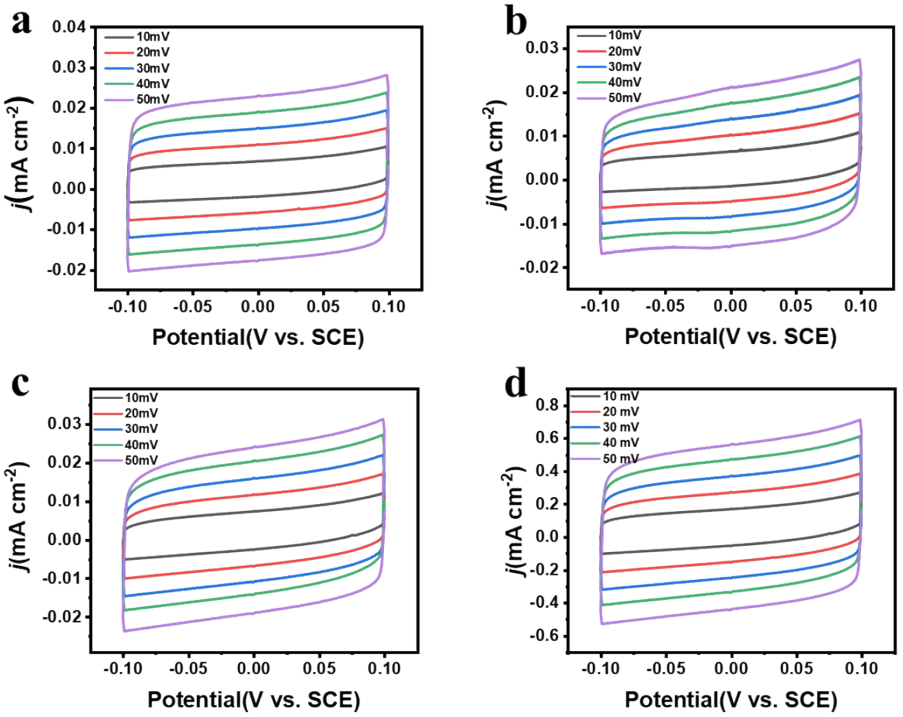

Figure S14. CV with different scan rate for Py-Bpy-Fe, Py-Bpy-Co, Py-Bpy-Ni and Py-PyIm-Fe.

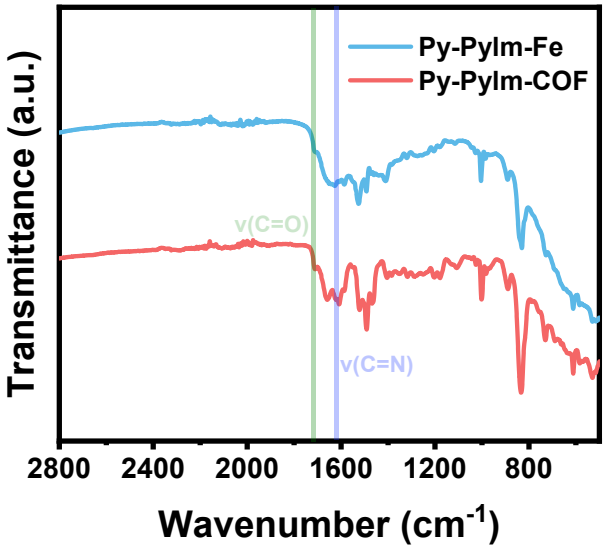

Figure S15. FT-IR spectra of Py-PyIm-COF and Py-PyIm-Fe.

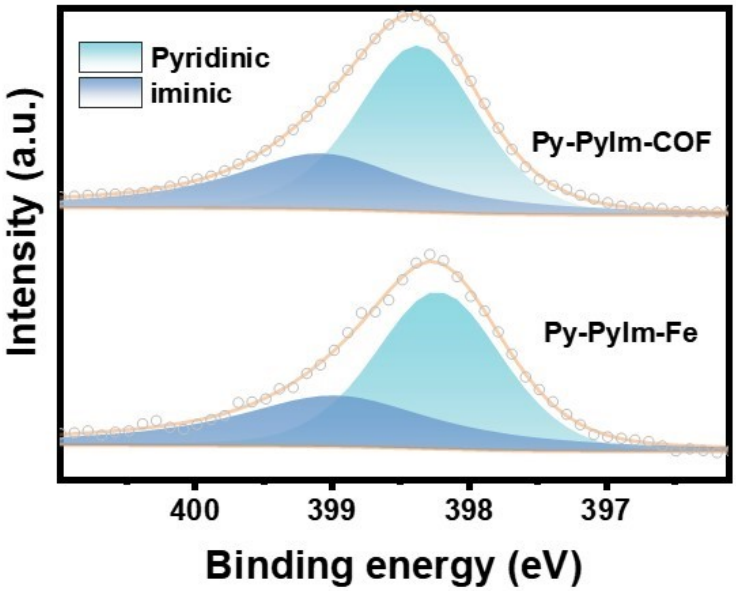

Figure S16. N 1s XPS spectra of Py-PyIm-COF and Py-PyIm-Fe.

Table S1. The comparison of electrocatalytic NO_3RR performance of Py-PyIm-Fe with other reported catalysts.

Catalyst	Electrolyte	NH_3 yield rate	FE_{max}(%)	Ref.
Py-PyIm-Fe	**1 M KOH/0.1 M KNO_3**	**4299.61 μmol h^{-1} mg^{-1}_{COF} at -2.0 V (vs. SCE)**	**86.8**	**This work**
Py-Bpy-Fe	**1 M KOH/0.1 M KNO_3**	**3909.06 μmol h^{-1} mg^{-1}_{COF} at -2.0 V (vs. SCE)**	**91.2**	**This work**
COF-366-Fe	0.5 M K_2SO_4/0.1 M KNO_3	1883.6 μmol h^{-1} mg^{-1}_{COF} at -1.7 V (vs. SCE)	85.4	[1]
NiPr-TPA-COF	0.5 M K_2SO_4/0.1 M KNO_3	2.5 mg h^{-1} cm^{-2} at -1.46V (vs. SCE)	90	[2]
Cu/JDC/CP	0.1 M NaOH/0.1 M NO_2	0.52 mmol h^{-1} mg^{-1}_{cat} at -0.6 V (vs. RHE)	93.2	[3]
Cu SAGs	0.1 M PBS/20 mM NO_3	0.44 mg h^{-1} cm^{-2} at -0.8 V (vs. RHE)	78	[4]
Fe SAC	0.1 M K2SO4/0.5 M KNO_3	5.24 mg h^{-1} mg^{-1}_{cat} at -0.66 V (vs. RHE)	75	[5]
Fe−N−C	0.05 M PBS/0.16 M NO_3	10 μmol h^{-1} cm^{-2} at -0.45 V (vs. RHE	82	[6]
Mo-N-C	0.05 M PBS/0.16 M NO_3	5 μmol h^{-1} cm^{-2} at -0.45 V (vs. RHE)	62	[6]
FeMo-N-C	0.05 M PBS/0.16 M NO_3	17 μmol h^{-1} cm^{-2} at -0.45 V (vs. RHE)	93	[6]

[1] H. Hu, R. Miao, F. Yang, F. Duan, H. Zhu, Y. Hu, M. Du, S. Lu, Intrinsic Activity of Metalized Porphyrin-based Covalent Organic Frameworks for Electrocatalytic Nitrate Reduction, Advanced Energy Materials, 14 (2024) 2302608.

[2] F. Lv, M. Sun, Y. Hu, J. Xu, W. Huang, N. Han, B. Huang, Y. Li, Near-unity electrochemical conversion of nitrate to ammonia on crystalline nickel porphyrin-based covalent organic frameworks, Energy & Environmental Science, 16 (2023) 201-209.

[3] L. Ouyang, L. Yue, Q. Liu, Q. Liu, Z. Li, S. Sun, Y. Luo, A.A. Alshehri, M.S. Hamdy, Q. Kong, Cu nanoparticles decorated juncus-derived carbon for efficient electrocatalytic nitrite-to-ammonia conversion, Journal of Colloid and Interface Science, 624 (2022) 394-399.

[4] J. Yang, H. Qi, A. Li, X. Liu, X. Yang, S. Zhang, Q. Zhao, Q. Jiang, Y. Su, L. Zhang, Potential-driven restructuring of Cu single atoms to nanoparticles for boosting the electrochemical reduction of nitrate to ammonia, Journal of the American Chemical Society, 144 (2022) 12062-12071.

[5] Z.-Y. Wu, M. Karamad, X. Yong, Q. Huang, D.A. Cullen, P. Zhu, C. Xia, Q. Xiao, M. Shakouri, F.-Y. Chen, Electrochemical ammonia synthesis via nitrate reduction on Fe single atom catalyst, Nature communications, 12 (2021) 2870.

[6] E. Murphy, Y. Liu, I. Matanovic, S. Guo, P. Tieu, Y. Huang, A. Ly, S. Das, I. Zenyuk, X. Pan, Highly durable and selective Fe-and Mo-based atomically dispersed electrocatalysts for nitrate reduction to ammonia via distinct and synergized NO_2–pathways, ACS Catalysis, 12 (2022) 6651-6662.